Electromagnetically and optomechanically induced transparency and amplification in an atom-assisted cavity optomechanical system

He Hao,[1] Mark C. Kuzyk,[2] Juanjuan Ren,[1] Fan Zhang,[1] Xueke Duan,[1] Ling Zhou,[3] Tiancai Zhang,[4,5]
Qihuang Gong,[1,5,6,7] Hailin Wang,[2] and Ying Gu ●[1,5,6,7,*]

[1]*State Key Laboratory for Mesoscopic Physics, Department of Physics, Peking University, Beijing 100871, China*
[2]*Department of Physics, University of Oregon, Eugene, Oregon 97403, USA*
[3]*School of Physics, Dalian University of Technology, Dalian 116024, China*
[4]*State Key Laboratory of Quantum Optics and Quantum Optics Devices, Institute of Opto-Electronics,*
Shanxi University, Taiyuan 030006, China
[5]*Collaborative Innovation Center of Extreme Optics, Shanxi University, Taiyuan, Shanxi 020006, China*
[6]*Nano-optoelectronics Frontier Center of the Ministry of Education and Collaborative Innovation Center of Quantum Matter,*
Peking University, Beijing, China
[7]*Beijing Academy of Quantum Information Sciences, Beijing 100193, China*

We propose an atom-assisted cavity optomechanical system consisting of a single Λ-type three-level atom, a mechanical resonator, and a sideband-driven cavity. The analytic expression of the system's evolution is constructed under the consideration of sideband-driven fields, then steady-state solution of electromagnetically and optomechanically induced transparency and amplification is presented. In the resolved red sideband case, we demonstrate the appearance of electromagnetically and optomechanically induced transparency when the two sets of two-photon resonances are satisfied. Moreover, we set up the eigenstate structure for this atom-assisted cavity optomechanical system, which gives an explicit explanation for the mechanism of the transparency. In the resolved blue sideband case, we can achieve the controllable amplification of the probe light, which is induced by the constructive interactions of photon, atom, and phonon. The proposed scheme offers insight for the tripartite coherent interaction among photons, atoms, and phonons, which will provide great flexibility for phonon storage and motivate the development of quantum information processing.

I. INTRODUCTION

Cavity quantum electrodynamics (CQED) has provided a ubiquitous platform for the interaction between atoms and photons at the single-photon level [1–3]. The well-established framework of cavity optomechanics interfaces photons to mechanical resonators [4–6]. Currently, motivated by the rapid development of quantum information networks, the combination of CQED and cavity optomechanics has been realized in photon-atom-phonon systems. These hybrid systems take advantage of each individual unit (e.g., the easy transportation of photons, the long coherence time of phonons, and the strong nonlinearity of atoms). Correspondingly, a wide range of physical phenomena appear, such as atom-assisted mechanical cooling [7], the all optically controlled phonon blockade [8], atom-enhanced photon-phonon coupling strength [9], the generation of nonclassical phonon states [10], and the analogous electromagnetically induced transparency (EIT) [11–13].

Since the first observation of EIT in atomic gases [14], the analogous EIT phenomenon has been realized in various systems, ranging from the CQED [15,16], to multimicrocavity systems [17], to cavity optomechanics [18–20]. More

recently, several works of the analogous EIT in atom-photon-phonon quantum systems have been presented by considering the tripartite interactions among them [11–13]. First, by introducing a qubit into an optomechanical system through mechanical strain, the qubit can be dressed with the mechanical mode and form the four-level-type structure. Thus, when a probe light propagates through the system accompanied by the red-detuned driven laser, the two-color transparency and tunable Fano resonance appear [12,13]. However, in these atom-assisted cavity optomechanical systems, the interaction between the qubit and the cavity field is not considered, leading to the loss of atomic EIT information. Another work demonstrates the multistability of atomic EIT in an optomechanical system [11]. Nevertheless, due to the resonant excitation of the cavity, the Stokes and anti-Stokes effects, induced by the interaction between the sideband-driven cavity and the mechanical mode, are neglected. The absence of such interactions prevents optomechanically induced transparency (OMIT) in these atom-assisted cavity optomechanical systems.

Here, taking the interaction between the atom and cavity fields into consideration as well as introducing the Stokes and anti-Stokes effects into the cavity optomechanics, we theoretically demonstrate electromagnetically and optomechanically induced transparency (EOMIT) and amplification (EOMIA) by integrating a single Λ-type three-level atom

(a)

(b)

(c)
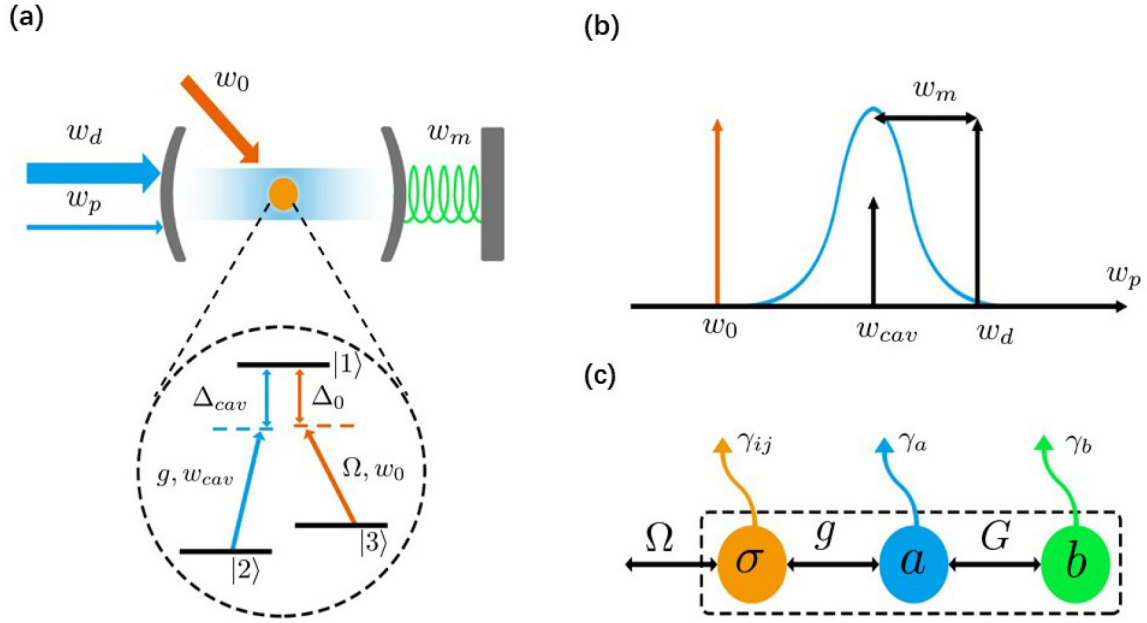
FIG. 1. (a) Schematic diagram of the atom-assisted cavity optomechanical system where a Λ-type three-level atom is placed inside an optical cavity. The cavity mode couples the transition $|2\rangle \leftrightarrow |1\rangle$ with the detuning $\Delta_{\text{cav}} = w_{12} - w_{\text{cav}}$ while the control field couples the transition $|3\rangle \leftrightarrow |1\rangle$ with the detuning $\Delta_0 = w_{13} - w_0$. (b) The driving lasers associated with the system where a laser at frequency w_d drives the cavity mode with red or blue detuning. (c) The coupling strength and decay rates in the atom-assisted cavity optomechanical system.

into the sideband-driven cavity ended with a movable mirror (see Fig. 1). The atom interacts with the cavity field of the optomechanical system as well as the classical, controllable light in the frame of CQED. Meanwhile, the cavity field, driven by a red-detuned or blue-detuned laser, interacts with the mechanical oscillator through radiation pressure. Based on the above considerations, we derive the analytic solution of the system evolution. In the resolved red sideband, we obtain the EOMIT in the form of the absorption and dispersion spectra of the probe light, where the transparent point accompanied by four symmetric peaks appears in the condition of two sets of two-photon resonances. To explain the mechanism of EOMIT, we set up the eigenstate structure. Furthermore, we find the properties of EOMIT (e.g., transparent point, width of transparency window) can be effectively tuned by several system parameters including the coupling strength between cavity field and atom, Rabi frequency of the atom, optomechanical cooperativity, as well as the relevant detunings. Finally, we discuss the EOMIA in the resolved blue sideband, which is induced by the constructive interaction among photon, atom, and phonon.

The innovation of our model lies in the combination of two kinds of interactions in the atom-assisted cavity optomechanical system: one is the interaction between the atom and the cavity mode, and the other is the interaction between the sideband-driven cavity mode and the mechanical mode. In other words, we can take advantage of both EIT and OMIT in the atom-assisted cavity optomechanical system. The main result of our work is the demonstration of the EOMIT, in which the width of the transparency window can be controlled by the coupling strength between the photons and the atom. The flexibility of control will bring potential applications in quantum information processing. For example, with the help

of EOMIT, the information carried by the atom can transfer to phonons through the photons. Moreover, due to additional tunable parameters induced by the atom such as coupling strength and Rabi frequency, the EOMIT makes it easier to generate slow light in cavity optomechanical experiments.

The paper is organized as follows. In Sec. II, we present the cavity optomechanical system and derive the analytic results of the system evolution. In Sec. III, we present the EOMIT and give the explicit explanation for the mechanism in the form of dressed states. Furthermore, we discuss the effects of various factors on EOMIT such as the coupling strength between cavity field and atom, the Rabi frequency, and optomechanical cooperativity. In Sec. IV, we demonstrate the EOMIA in the resolved blue sideband. Finally, we summarize our results in Sec. V.

II. ATOM-PHOTON-PHONON MODEL SETUP

A. Hamiltonian

As schematically shown in Fig. 1(a), an atom-assisted cavity optomechanical system is considered, where a Λ-type three-level atom is placed inside the optical cavity. The atom's excited and ground states are labeled as $|1\rangle$ and $|2\rangle$, $|3\rangle$. The atomic transition $|1\rangle \leftrightarrow |2\rangle$ with energy-level difference $w_{12} = w_1 - w_2$ is coupled to the cavity mode of frequency w_{cav}. Their frequency detuning is $\Delta_{\text{cav}} = w_{12} - w_{\text{cav}}$ and g represents their coupling strength. The transition $|1\rangle \leftrightarrow |3\rangle$ is driven by a classical, controllable field of frequency w_0 with Rabi frequency Ω and detuning $\Delta_0 = w_{13} - w_0$. The interaction between the cavity mode and the mechanical resonator is described by radiation pressure with coupling strength G, where the frequency of the mechanical resonator is w_m. The cavity mode is driven by a strong laser of frequency w_d,

which will be set at the red or blue sideband according to the corresponding needs. Figure 1(b) schematically shows the frequency of the cavity mode and driving fields mentioned above. Notably, the controllable laser w_0 is away from w_{cav} (i.e., it does not excite the cavity mode). Meanwhile, we also ignore the three-body interaction by moving the position of the atom slightly away from the maximum of the electric field; thus, the coupling strength between the cavity field and the atom changes little as the cavity length varies in time [21,22]. Consequently, as shown in Fig. 1(c), there are three interactions in the atom-assisted cavity optomechanical system (i.e., photons interact with phonons via the radiation pressure while photons interface with atoms under the CQED framework), and there is interaction between atoms and the external field additionally.

Under the dipole and rotating wave approximation consideration, the Hamiltonian of the total system reads

$$H = H_0 + H_{\text{AC}} + H_{\text{CM}} + H_{\text{dri}}, \tag{1}$$

where $H_0 = \hbar w_1 \sigma_{11} + \hbar w_2 \sigma_{22} + \hbar w_3 \sigma_{33} + \hbar w_{\text{cav}} a^+ a + \hbar w_m b^+ b$ with $\sigma_{ii} = |i\rangle\langle i|$ ($i = 1, 2, 3$). The operators a and b are the annihilation operators of the cavity mode and the mechanical mode, respectively. The second term can be written as $H_{\text{AC}} = \hbar(\Omega \sigma_{13} e^{-i w_0 t} + g a \sigma_{12} + \text{H.c.})$, describing the interaction between the atom and the classical as well as the cavity mode. The third term is $H_{\text{CM}} = -\hbar G a^+ a(b + b^+)$, which represents the interaction between the mechanical resonator and the cavity field. The final term is given by $H_{\text{dri}} = i\hbar\sqrt{2\eta\gamma_a}[(\varepsilon_d a^+ e^{-i w_d t} - \varepsilon_d^* a e^{i w_d t}) + (\varepsilon_p a^+ e^{-i w_p t} - \varepsilon_p^* a e^{i w_p t})]$, where ε_d and ε_p describe the strength of the driven and probe light with power $P_j = \frac{\hbar w_j \varepsilon_j^2}{2\eta\gamma_a}$ incident on the cavity. The coupling parameter is $\eta = \frac{\gamma_{ex}}{\gamma_a}$, where γ_a denotes the cavity loss rate and γ_{ex} the external decay rate.

Introducing the rotating wave approximation, the Hamiltonian of the hybrid system is given by

$$\begin{aligned}
H_I &= \hbar\Delta_{\text{cav}}\sigma_{11} + \hbar(\Delta_{\text{cav}} - \Delta_d)\sigma_{22} + \hbar(\Delta_{\text{cav}} - \Delta_0)\sigma_{33} \\
&+ \hbar(\Delta_d - \Delta_{\text{cav}})a^+ a + \hbar w_m b^+ b - \hbar G a^+ a(b + b^+) \\
&+ \hbar(\Omega\sigma_{13} + g a\sigma_{12} + \text{H.c.}) + i\hbar\sqrt{2\eta\gamma_a}[(\varepsilon_d a^+ - \varepsilon_d^* a) \\
&+ (\varepsilon_p a^+ e^{i(\Delta_p - \Delta_d)t} - \varepsilon_p^* a e^{-i(\Delta_p - \Delta_d)t})], \tag{2}
\end{aligned}$$

where the detunings are defined as $\Delta_p = w_{12} - w_p$, $\Delta_d = w_{12} - w_d$. If we ignore the atomic items in Eq. (2), the Hamiltonian will degenerate to the results of OMIT [18]. The difference lies in that we introduce the optically controlled atom under the framework of CQED, which provides the interaction between atom and photons. If we assume that both of the cavity mirrors are fixed, Eq. (2) will converge to the Hamiltonian which describes the cavity-induced EIT [15]. Consequently, our model has a distinct feature: it involves the sideband-driven cavity and the optically controlled atom simultaneously, which allows us to combine the Stokes or anti-Stokes effects together with the atom.

B. Heisenberg-Langevin equations

Substituting Eq. (2) into the Heisenberg-Langevin equations of motion and introducing the corresponding damping

terms phenomenologically, we have

$$\begin{aligned}
\dot{a} &= -[\gamma_a + i(\Delta_d - \Delta_{\text{cav}}) - iG((b + b^+)]a - ig^*\sigma_{21} \\
&+ \sqrt{2\eta r_a}\varepsilon_d + \sqrt{2\eta r_a}\varepsilon_p e^{i(\Delta_p - \Delta_d)t} + f_a, \\
\dot{b} &= -(\gamma_m + i w_m)b + iGa^+ a + f_b, \\
\dot{\sigma}_{21} &= -(\gamma_{12} + i\Delta_d)\sigma_{12} + iga(\sigma_{11} - \sigma_{22}) - i\Omega\sigma_{23} + f_{21}, \\
\dot{\sigma}_{23} &= -[\gamma_{32} + i(\Delta_d - \Delta_0)]\sigma_{23} - i\Omega^*\sigma_{21} + f_{23}, \tag{3}
\end{aligned}$$

where γ_a, γ_m, γ_{12}, and γ_{32} are the decay rates of the cavity mode, mechanical mode, and the atom, respectively. And f_a, f_b, f_{21}, and f_{23} are corresponding quantum and thermal noises in each term.

In the following, we linearize the Heisenberg-Langevin equations under the condition of $\varepsilon_d \gg \varepsilon_p$, in which the Heisenberg operator can be rewritten as a sum of its steady-state mean value plus its small fluctuation [4,11], i.e., $a = \bar{a} + \delta a$, $b = \bar{b} + \delta b$, $\sigma_{21} = \overline{\sigma_{21}} + \delta\sigma_{21}$, and $\sigma_{23} = \overline{\sigma_{23}} + \delta\sigma_{23}$. Furthermore, the atom is initially prepared in the ground state $|2\rangle$. Thus, $\langle\sigma_{11}\rangle = \langle\sigma_{33}\rangle = \langle\sigma_{13}\rangle = \langle\sigma_{31}\rangle = 0$. The steady-state mean value for the cavity mode and the mechanical mode can be obtained by setting all the time derivatives in Eqs. (3) to be zero:

$$\begin{aligned}
\bar{b} &= \frac{iG\bar{a}^2}{\gamma_m + i w_m}, \\
\bar{a} &= \frac{\sqrt{2\eta\gamma_a}\varepsilon_d}{\gamma_a + i\Delta' + \frac{g^2}{\gamma_{12} + i\Delta_d + \frac{\Omega^2}{\gamma_{32} + i(\Delta_d - \Delta_0)}}}, \tag{4}
\end{aligned}$$

where $\Delta' = \Delta_d - \Delta_{\text{cav}} - iG((\bar{b} + \bar{b}^*)$ (details are shown in the Appendix). For the fluctuation part, we neglect the high-order small terms ($\delta a^+ \delta a$) as being smaller by a factor $\bar{a}$ and obtain its time derivatives:

$$\begin{aligned}
\dot{\delta a} &= -(\gamma_a + i\Delta')\delta a + iG\bar{a}(\delta b + \delta b^+) - ig^*\delta\sigma_{21} \\
&+ \sqrt{2\eta r_a}\varepsilon_p e^{i(\Delta_p - \Delta_d)t} + f_a, \\
\dot{\delta b} &= -(\gamma_a + i w_m)\delta b + iG(\bar{a}^*\delta a + \bar{a}\delta a^+) + f_b, \\
\dot{\delta\sigma}_{21} &= -(\gamma_{12} + i\Delta_d)\delta\sigma_{21} - ig\delta a - i\Omega\delta\sigma_{23} + f_{21}, \\
\dot{\delta\sigma}_{23} &= -[\gamma_{32} + i(\Delta_d - \Delta_0)]\delta\sigma_{23} - i\Omega^*\delta\sigma_{21} + f_{23}. \tag{5}
\end{aligned}$$

According to the methods in Refs. [18,19], we identify all operators with their expectation values and drop the quantum and thermal noises, i.e., $y \equiv \langle y\rangle$ (where y denotes δa, δb, $\delta\sigma_{21}$, and $\delta\sigma_{23}$). To analyze the response of the system, we solve the equations of the expectation values using the ansatz $y = y_+ e^{i(\Delta_p - \Delta_d)t} + y_- e^{-i(\Delta_p - \Delta_d)t}$, which applies to the parameter ε_p to first order [18,19]. Up to now, we have set up the Hamiltonian of the atom-assisted cavity optomechanical system and derived the evolution of each operator. In the following, we give explicit results with driving laser w_d at red-detuned frequency or blue-detuned frequency.

III. ELECTROMAGNETICALLY AND OPTOMECHANICALLY INDUCED TRANSPARENCY

In this section, we study the cavity response to the probe light under the resolved red sideband regime. We give the analytic results for the system evolution, and demonstrate a transparent point and the symmetric absorption spectra

in the condition of two sets of two-photon resonances. To reveal the mechanism of EOMIT and explain the formation of the absorption spectra, the eigenstate structure for the atom-assisted cavity optomechanical system is set up. We also show the influence of several system parameters on the EOMIT, including the coupling strength between cavity field and atom, Rabi frequency of the atom, and the optomechanical cooperativity.

A. System evolution

By placing the driven field w_d at red-detuned frequency (i.e., $\Delta_d - \Delta_{cav} \approx w_m$), we ignore the terms $iG\bar{a}\delta b^+$ and $iG\bar{a}\delta a^+$ in Eqs. (5) due to the rotating wave approximation. Thus, using the methods in Ref. [19], we can only consider one sideband of the intracavity photons (δa_-) because the other part is nearly zero. Subsequently, we obtain

$$\delta\sigma_{23} = \frac{-i\Omega^*\gamma_{32} + i(\Delta_p - \Delta_0)}{\delta}\sigma_{21}, \quad \delta\sigma_{21} = \frac{-ig}{\gamma_{12} + i\Delta_p + \frac{\Omega^2}{\gamma_{32}+i(\Delta_p-\Delta_0)}}\delta a, \quad \delta b = \frac{iG\bar{a}^*}{\gamma_m + i(w_m + \Delta_p - \Delta_d)}\delta a,$$

$$\delta a = \frac{\sqrt{2\eta r_a}\varepsilon_p}{\gamma_a + i(\Delta' + \Delta_p - \Delta_d) + \frac{G^2\bar{a}^2}{\gamma_m+i(w_m+\Delta_p-\Delta_d)} + \frac{g^2}{\gamma_{12}+i\Delta_p+\frac{\Omega^2}{\gamma_{32}+i(\Delta_p-\Delta_0)}}}. \tag{6}$$

Equations (6) are the main result of EOMIT, from which we can see that there is a transparent point as long as the two-photon resonance condition, $\Delta_d - \Delta_p = w_m$, is met. Notably, to obtain the results of EOMIT, we neglect the three-body interaction in the system, prepare the atom at its ground state, and make the standard linearization of the optomechanical interaction. Also, we drive the system in the resolved red-detuning regime; thus, the omission of the Stokes effect of the intracavity photons is reasonable. The transparent point can also be obtained in the work of OMIT under the same condition [20]. However, the transparent point here can be controlled by the coupling strength g and Rabi frequency Ω, providing more flexibility in experiments. Additionally, when another set of two-photon resonance conditions, $\Delta_p = \Delta_{cav} = \Delta_0$, is met simultaneously, the absorption spectrum is on symmetry of the transparent points.

In the following, we consider the characteristics of EOMIT under the two sets of two-photon resonance conditions. According to the input-output theory [23] for the open quantum system, the output field follows the relation $\frac{\varepsilon_{out}}{\sqrt{2\eta\gamma_a}} + \frac{\varepsilon_p}{\sqrt{2\eta\gamma_a}} = \delta a = \varepsilon_T\varepsilon_p$. We redefine the output field as $\varepsilon_T = \sqrt{2\eta\gamma_a}\frac{\delta a}{\varepsilon_p}$ with the real and imaginary parts $u_p = \frac{\sqrt{2\eta\gamma_a}}{2\varepsilon_p}(\delta a + \delta a^*)$ and $v_p = \frac{\sqrt{2\eta\gamma_a}}{2i\varepsilon_p}(\delta a - \delta a^*)$. It is clear that u_p and v_p describe absorption and dispersion of the probe field [12].

Figure 2(a) plots the absorption and dispersion spectra of probe light as a function of detuning Δ_p with $\Delta_d = w_m$ and $\Delta_0 = \Delta_{cav} = 0$. The parameters are set as $\gamma_a = 1$ MHz, $g = \gamma_a$, $\Omega = 2\gamma_a$, $\gamma_{12} = 0.5\gamma_a$, $\gamma_{32} = \gamma_m = 0.01\gamma_a$, $\eta = 0.6$, and the optomechanical cooperativity $C = \frac{G^2\bar{a}^2}{\gamma_a\gamma_m} = 4$, which partially references the experimental data [16,19]. Compared with the absorption of an empty cavity [dashed line in Fig. 2(a)], there is a transparent point located at $\Delta_p = 0$ and four symmetric absorption peaks located at $-2.29\gamma_a$, $-0.18\gamma_a$, $0.18\gamma_a$, and $2.29\gamma_a$, respectively. Meanwhile, each peak and the transparent point lead to a steeper slope in the dispersion spectrum. This effect can be used for reducing the group velocity of the probe light, making it an important building block in quantum information and communication proposals, as well as of great practical interest in classical optics and photonics [24,25].

B. Eigenstates structure

Now, we start to reveal the mechanism of EOMIT. At the beginning, it is instructive to emphasize the origin of both OMIT and the standard EIT using the dressed state language. Considering the Λ-type three-level atom under the two-photon resonance condition [$\Delta_{cav} = \Delta_0$ in Fig. 1(a)], the control light couples the states $|1\rangle$ and $|3\rangle$, leading to two dressed states $|\pm\rangle = \frac{1}{\sqrt{2}}(|1\rangle \pm |3\rangle)$, which effectively decay to the same ground state $|2\rangle$ [14]. This would result in a transparent point in the absorption spectrum. Similarly, the energy-level diagram for OMIT can be understood as a Λ-type three-level system formed by three states $|n_p, n_m\rangle$, $|n_p + 1, n_m\rangle$, and $|n_p, n_m + 1\rangle$, where $|n_p\rangle$ and $|n_m\rangle$ represent the number states of the cavity and mechanical modes, respectively. Under the two-photon resonance, i.e., $w_p - w_d = w_m$, the OMIT appears with a transparent point, which is induced by the two dressed states $|\oplus, \ominus\rangle = \frac{1}{\sqrt{2}}(|n_p + 1, n_m\rangle \pm |n_p, n_m + 1\rangle)$ coupling to the same ground state $|n_p, n_m\rangle$ [20].

Considering the atom-assisted cavity optomechanical system, it evolves in a discrete but infinite Hilbert space in which the uncoupled eigenvectors are labeled as $\{|n_p\rangle \otimes |n_m\rangle \otimes |i\rangle\}$. Each subspace contains exactly N excitations (atom, photon, or phonon). For the ground state $N = n_p + n_m$, there is no excitation in the atom and the new dressed states can be written as $\psi_0 = |2, n_p, n_m\rangle$. For $N = n_p + n_m + 1$, there is one more excitation in the system, rewriting the Hamiltonian in the new basis $\{|2, \oplus n_m\rangle, |2, \ominus n_m\rangle, |+, n_p n_m\rangle, |-, n_p n_m\rangle\}$ and for $w_m + \Delta_p - \Delta_d = 0$ and $\Delta_p = \Delta_0 = \Delta_{cav} = 0$, yields the four eigenstates, ψ_1, ψ_2, ψ_3, and ψ_4 with the following eigenvalues:

$$E_1 = -\frac{\sqrt{2}}{2}\sqrt{g^2 + \Omega^2 + G^2\bar{a}^2 + z}, \tag{7}$$

$$E_2 = -\frac{\sqrt{2}}{2}\sqrt{g^2 + \Omega^2 + G^2\bar{a}^2 - z}, \tag{8}$$

$$E_3 = \frac{\sqrt{2}}{2}\sqrt{g^2 + \Omega^2 + G^2\bar{a}^2 - z}, \tag{9}$$

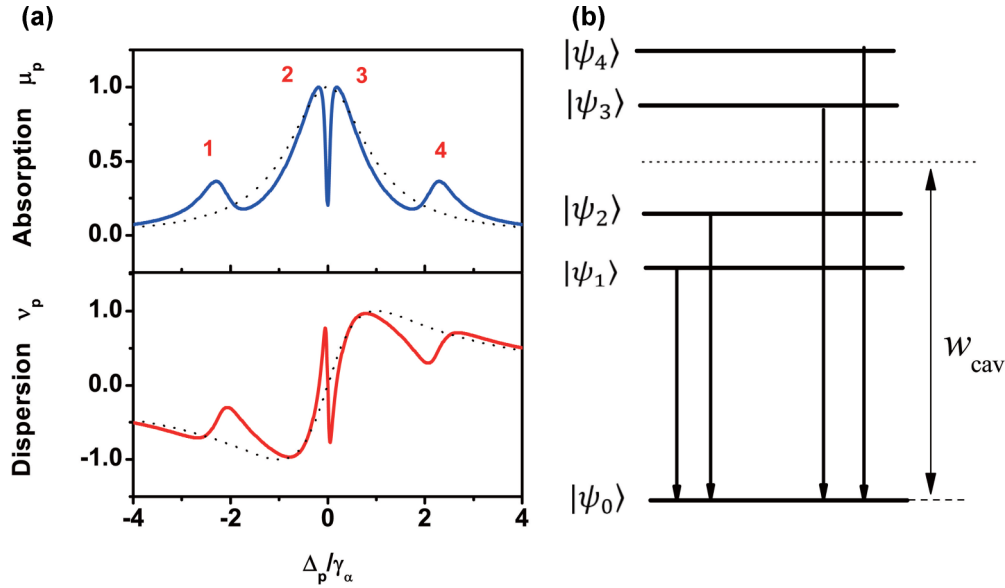$$E_4 = \frac{\sqrt{2}}{2}\sqrt{g^2 + \Omega^2 + G^2\bar{a}^2 + z}, \tag{10}$$

FIG. 2. Electromagnetically and optomechanically induced transparency. (a) Absorption and dispersion spectra of probe light as a function of detuning Δ_p. The transparent point appears at $\Delta_d = w_m$, and there are four symmetric peaks under the two sets of two-photon resonance conditions $\Delta_d = w_m$ and $\Delta_0 = \Delta_{\text{cav}} = 0$ (dashed black line shows the absorption of the cavity without the atom and mechanical oscillator). Both peaks and transparent points lead to steep slopes in the dispersion spectrum. Other parameters here are $g = \gamma_a$, $\Omega = 2\gamma_a$, C = 4, $\gamma_{12} = 0.5\gamma_a$, and $\gamma_{32} = \gamma_m = 0.01\gamma_a$. (b) The eigenstate structure for the atom-assisted cavity optomechanical system. Each eigenstate in $(N + 1)$-excitation subspace couples independently to the ground state in N-excitation subspace with different displacements, corresponding to the four peaks in the absorption spectrum.

where $z = \sqrt{g^4 + G^4\bar{a}^4 + \Omega^4 + 2g^2G^2\bar{a}^2 + 2g^2\Omega^2 - 2G^2\bar{a}^2\Omega^2}$. Similar to the standard EIT system, these eigenstates compose an anharmonic ladder structure as shown in Fig. 2(b), and they decay to the same state $\psi_0 = |2, n_p, n_m\rangle$. Thus, the transparent point appears as long as the two sets of two-photon resonances are fulfilled, i.e., $w_m + \Delta_p - \Delta_d = 0$ and $\Delta_p = \Delta_0 = \Delta_{\text{cav}} = 0$. It is important to note that the transparent point would appear when $w_m + \Delta_p - \Delta_d = 0$. The other condition $\Delta_p = \Delta_0 = \Delta_{\text{cav}} = 0$ guarantees that the spectrum is symmetric. The four peaks in the absorption spectrum correspond to an energy-level difference $E_x - E_y$ $(x, y \in (1, 2, 3, 4))$. Using the parameters in Fig. 2(a), we get the four peaks at $-2.25\gamma_a$, $-0.15\gamma_a$, $0.15\gamma_a$, and $2.25\gamma_a$, which is in accordance with the numerical results. It is noteworthy that each eigenvalue can be affected by the coupling strength between cavity field and atom, the Rabi frequency of the atom, and the optomechanical cooperativity, providing more degrees of freedom than EIT and OMIT systems, which are given in detail in the following part.

C. Effects of parameters on EOMIT

Generally speaking, the properties of the EOMIT depend on several system parameters, such as coupling strength g, Rabi frequency Ω of the atom, optomechanical cooperativity C, as well as relevant detunings. In this part, we demonstrate the relationship between these parameters and EOMIT. First, we plot the absorption and dispersion of the probe field for different values of the coupling strength g for $\Omega = \gamma_a$ and C = 100. When $g = 0$, there are two peaks in the absorption spectrum, accompanied by a transparent point located at $\Delta_p =$

0. Increasing the coupling strength g, as Fig. 3(a) shows, each peak splits into two separated peaks, and the whole absorption is symmetric on the transparency point. In this process, the width of the transparency windows becomes narrower while the transparent point remains at the same location. The numerical values agree with the eigenstate structure theory and we refer to the phenomenon as analogous atom Rabi splitting [26]. Moreover, all peaks and the transparent point are accompanied by a steep slope in the dispersion spectra. As shown in Fig. 3(a), the slope becomes steeper when g increases from 0 to $2\gamma_a$. Therefore, the group velocity for the probe light can be controlled by changing the coupling strength g. The larger the value of g, the slower the group velocity of the probe light [24,25]. Notably, it is instructive to show the difference between the OMIT and EOMIT. For OMIT, the width of the transparency window depends only on the cavity cooperativity C [18]. But, for EOMIT, the width of the transparency window can be modulated not only by the cavity optomechanical system but also by the atomic parameters.

The spectrum of EOMIT can also be affected by the cavity cooperativity C. Figure 4(a) shows the absorption u_p versus the probe light with various C under the parameters $\Omega = 2\gamma_a$ and $g = \gamma_a$. When C increases from C = 4 via C = 25 to C = 100, the location of peaks labeled as 2 and 3 changes from $\pm 0.18\gamma_a$ via $\pm 1.21\gamma_a$ to $\pm 1.54\gamma_a$, resulting in the widening of the transparency window. Here, the position of peaks labeled as 1 and 4 changes a little, from $\pm 2.29\gamma_a$ via $\pm 2.43\gamma_a$ to $\pm 2.65\gamma_a$. The results are coincident with the predicted results of the eigenstate structure. However, the transparent point remains the same as long as $\Delta_d - \Delta_p = w_m$ and the spectrum is symmetric when $\Delta_{\text{cav}} = \Delta_0$.
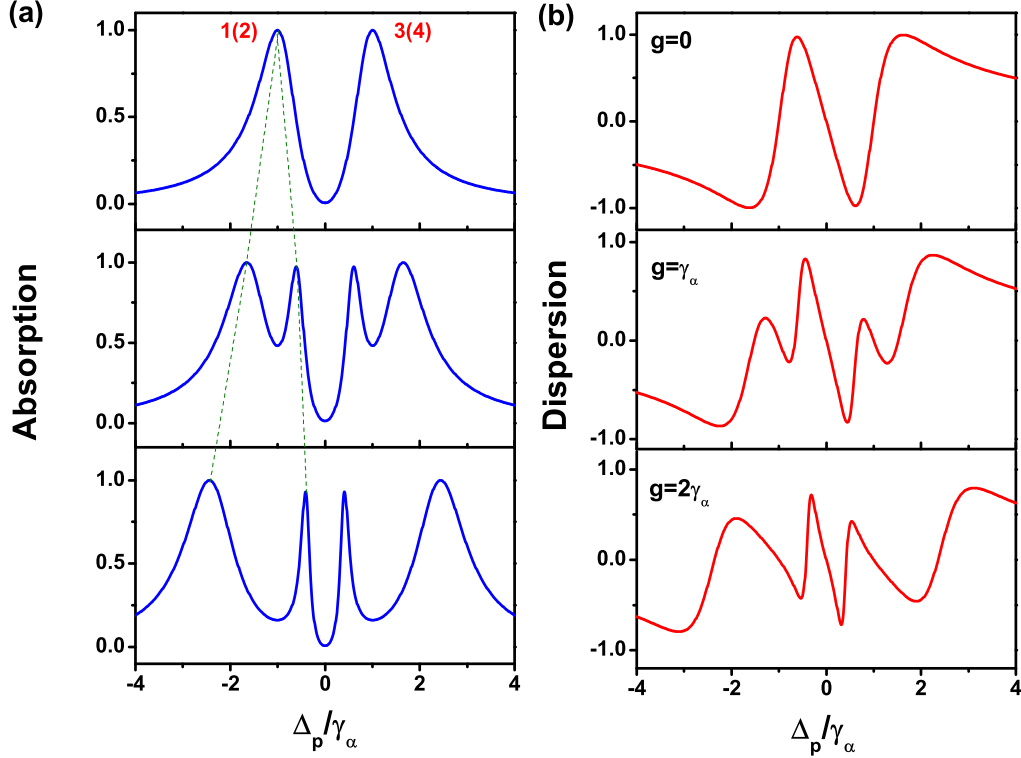
FIG. 3. (a) The absorption spectra and (b) dispersion spectra for a probe light under different coupling strength g. When $g = 0$, there are two peaks in the absorption spectrum; with the increase of g, each peak splits into two peaks, leading to a narrower transparency window. In the process, the transparent point remains the same as long as $\Delta_p = 0$. Here, $\Omega = \gamma_a$, C $= 100$, and the other parameters are the same as those in Fig. 2(a).

It can be seen from Eqs. (6) that the Rabi frequency Ω can also influence the feature of EOMIT. As shown in Fig. 4(b), we plot the absorption u_p versus detuning Δ_p at different Rabi frequencies Ω under the same parameters where $g = \gamma_a$ and C $= 100$. When $\Omega = 0$, there are two peaks located at $\pm 1.36\gamma_a$ in the absorption spectrum and the transparent point remains at $\Delta_p = 0$. With increasing Ω, there are another two new peaks appearing in the absorption spectrum and the old ones move further away from the transparent point. When $\Omega = 2\gamma_a$, the positions for the four peaks are $-2.33\gamma_a$, $-0.83\gamma_a$, $0.83\gamma_a$, and $2.33\gamma_a$, while the transparent point remains in the same location. We can find the reason from the eigenstate results. When $\Omega = 0$, two of the eigenstates are equal to zero, resulting in the coincidence between the absorption peaks and the transparent point.

We also study the effects of relevant detunings to EOMIT. The spectrum will be asymmetric when the condition $\Delta_{cav} = \Delta_0$ is not satisfied. We show that the peaks will redshift when $(\Delta_{cav}, \Delta_0) > 0$. The position of the transparent point changes significantly when there is a mismatch between $\Delta_d - \Delta_p$ and w_m.

Up to now, we have shown that the transparency point can be tuned by the relevant detunings and the width of the transparency window can be increased by decreasing the coupling strength between the cavity field and atom or increasing the Rabi frequency of the atom and optomechanical cooperativity. The EOMIT plays an important role in quantum state transduction and quantum memory. For example, the information carried by the atom can be transferred to a phonon with the help of the photon, which has long coherence time and can be an ideal carrier for quantum memory. Also, the EOMIT has the potential to generate slow light as the width of the transparency window can be controlled by Rabi frequency, which is easy to implement in experiments.

IV. ELECTROMAGNETICALLY AND OPTOMECHANICALLY INDUCED AMPLIFICATION

In this section, we consider the case when the cavity is driven in the resolved blue-detuned regime. By placing the driven field with frequency w_d at $\Delta_d - \Delta_{cav} \approx w_m$, similar to Sec. III, we may ignore the terms $iG\bar{a}\delta b$ and $iG\bar{a}\delta a$ in Eqs. (5) and only consider the δa_+ sideband of the intracavity photons.

Consequently, we obtain the intracavity field as

$$\delta a = \frac{\sqrt{2\eta\gamma_a}\varepsilon_p}{\gamma_a + i(\Delta' + \Delta_p - \Delta_d) + \dfrac{G^2\bar{a}^2}{-\gamma_m + i(w_m - \Delta_p + \Delta_d)} + \dfrac{g^2}{\gamma_{12} + i\Delta_p + \dfrac{\Omega^2}{\gamma_{32} + i(\Delta_p - \Delta_0)}}}. \tag{11}$$
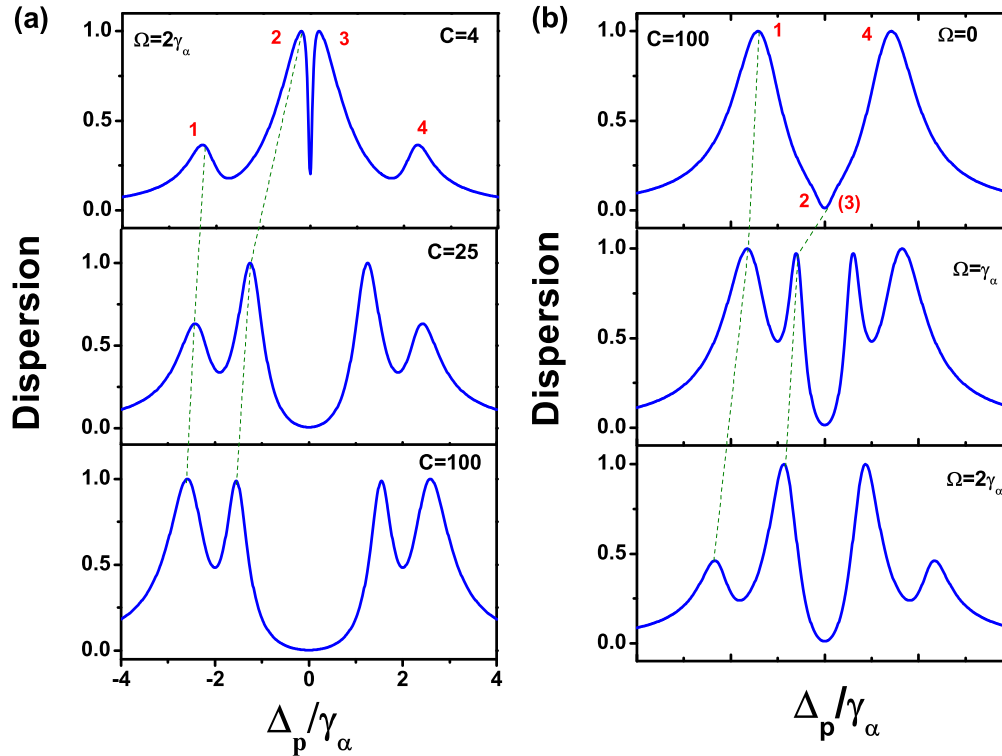
FIG. 4. The absorption spectra for the probe light for (a) different cavity cooperativity and (b) different Rabi frequency. The width of the transparency window becomes wide with the increase of C or Ω. The transparent point remains as long as $\Delta_d - \Delta_p = w_m$ while the spectrum is symmetric when $\Delta_{cav} = \Delta_0$. Here, $\Omega = 2\gamma_a$, $g = \gamma_a$ for (a) and $g = \gamma_a$, C = 100 for (b), and the other parameters are the same as those in Fig. 2(a).

The valid range of the result is similar to those of EOMIT, i.e., omitting the three-body interaction, making the standard linearization and preparing the atom at its ground state, except

that the driving laser is in the resolved blue-detuning regime. We define the amplification of the probe light as $P_{out}/P_{in} = \varepsilon_T^2$. Using the parameters C = 0.4, $\gamma_{12} = 0.5\gamma_a$, and $\gamma_{32} =$
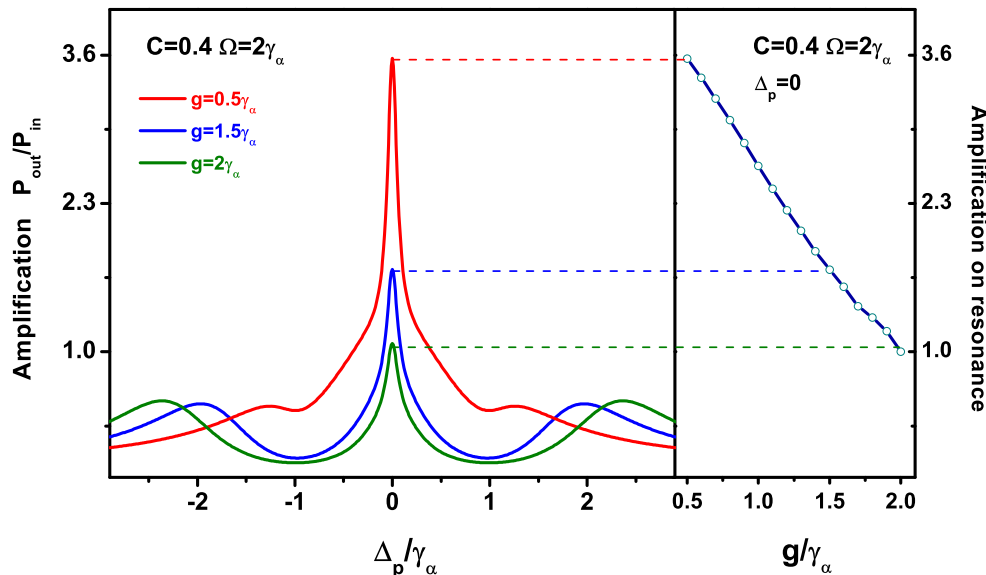

FIG. 5. Electromagnetically and optomechanically induced amplification. The amplification of the probe light for three different coupling strengths g from $0.5\gamma_a$ to $2\gamma_a$ (corresponding to the curves from up to bottom in the figure). The maximum value of amplification on resonance ($\Delta_p = 0$) directly indicates the maximum probe power transmission achieved in this case. These values are given in the right-hand panel for a large scan of g, representing the linear relationship between the amplification and g. Here, $\Omega = 2\gamma_a$, C = 0.4, $\Delta_p - \Delta_d = w_m$, and the other parameters are the same as those in Fig. 2(a).
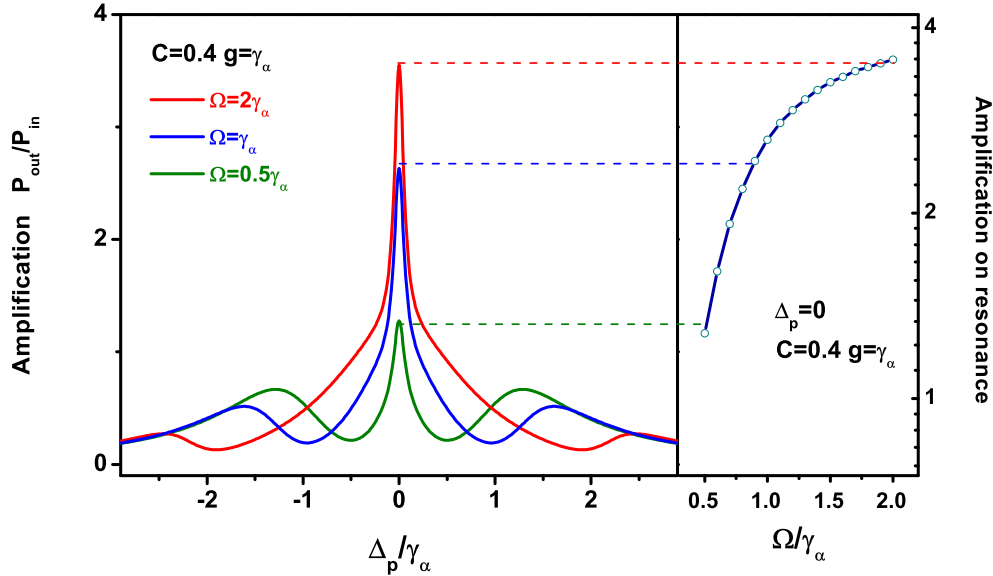
FIG. 6. The amplification of probe light for three different values of Rabi frequency Ω from $0.5\gamma_a$ to $2\gamma_a$ (corresponding to the curves from bottom to up in the figure). The maximum value of amplification on resonance ($\Delta_p = 0$) directly indicates the maximum probe power transmission achieved in this case. These values are given in the right-hand panel for a large scan of Ω, representing the nonlinear relationship between the amplification and Ω. Here, $g = \gamma_a$, C = 0.4, and the other parameters are the same as those in Fig. 2(a).

$\gamma_m = 0.1\gamma_a$, we calculate the amplification of the probe light under different coupling strength g and Rabi frequency Ω.

Different from EOMIT, when the probe light propagates through the system under the blue sideband driven case, it will be amplified due to the constructive interaction between the photon, atom, and phonon. When $\Delta_p - \Delta_d = w_m$, the coherent interaction between phonons and photons will cause the amplification of the probe light, referred to as optomechanically induced amplification [27,28]. Meanwhile, due to the satisfaction of two-photon resonance $\Delta_{\text{cav}} = \Delta_0$ for EIT, the amplification will compete with the absorption, leading to the atom-controllable amplification, called EOMIA. Figure 5 plots the trace of amplification $P_{\text{out}}/P_{\text{in}} = \varepsilon_T^2$ under the different values of coupling strength g. The maximum amplification is set by injecting the probe light on resonance ($\Delta_p = 0$), whose values are given in the right-hand panel for a large scan of g. When g is small, the absorption effect induced by cavity EIT is weakened, so the amplification will be large (e.g., the power of the output light will be amplified by a factor of 3.5 when $g = 0.5\gamma_a$). Increasing the value of g, the absorption effect can suppress amplification, and the threshold for the balance of input and output energy occurs when $g = 2\gamma_a$. Under this condition, the energy of output light is equal to the input light.

Moreover, we plot the amplification of the probe light under different values of Rabi splitting Ω in Fig. 6. With increased values of Ω, the amplification will also become large. When $\Omega = 0.5\gamma_a$, the amplification is 1.27 while the amplification is 3.5 when $\Omega = 2\gamma_a$. The relationship between $P_{\text{out}}/P_{\text{in}}$ and Ω is nonlinear, as shown in the right-hand panel of Fig. 6, the amplification will tend to be stable when Ω is larger than $2\gamma_a$. Clearly, we will not obtain a larger amplification compared with optomechanically induced amplification [27,28], but we introduce the flexibility into this

process; i.e., we can modulate the amplification through the Rabi frequency and the coupling strength between atom and cavity mode. If we combine this idea with active quantum devices, it will play roles in quantum modulators [29] or even switches [30] with the help of state-of-the-art preparation technology.

V. CONCLUSION

In summary, we have demonstrated electromagnetically and optomechanically induced transparency (EOMIT) and electromagnetically and optomechanically induced amplification (EOMIA) in an atom-assisted cavity optomechanical system, which consists of a sideband-driven cavity, Λ-type three-level atom, and mechanical oscillator. We have constructed the analytic expression of system evolution under the atom-photon-phonon coherent interaction. Based on these tripartite interactions, we have proposed the EOMIT in the red resolved sideband where the transparent point appears under the condition of one set of two-photon resonance while the absorption spectrum is symmetric in the condition of another set of two-photon resonance. To reveal the mechanism for EOMIT, we have set up an eigenstate structure for the atom-assisted cavity optomechanical system. We have also shown the influence of various factors on EOMIT, including the coupling strength between cavity field and atom, Rabi frequency, and optomechanical cooperativity, as well as relevant detunings. Furthermore, we have obtained the EOMIA in the blue resolved sideband, where the amplification can be controlled by the coupling strength and Rabi frequency.

We hope that our study, in particular the finding of EOMIT and EOMIA, might provide some new insight for the combination of cavity quantum electrodynamics and cavity

optomechanics by integrating a three-level atom into a sideband-driven optomechanical cavity. The atom-assisted cavity optomechanical scheme would bring great flexibility for manipulating light, which can be used for generating slow light and amplifying signal light. In terms of the applications in quantum information processing, the EOMIT provides a scheme for phonon storage which can be mediated by atomic Rabi frequency and coupling strength, while the EOMIA could be an element for a quantum switch.

APPENDIX

Under the condition of $\varepsilon_d \gg \varepsilon_p$, the Heisenberg operator can be rewritten as a sum of its steady-state mean value plus its small fluctuation, i.e., $a = \bar{a} + \delta a$, $b = \bar{b} + \delta b$, $\sigma_{21} = \overline{\sigma_{21}} + \delta\sigma_{21}$, and $\sigma_{23} = \overline{\sigma_{23}} + \delta\sigma_{23}$. For the mean-value part, we have

$$\dot{\bar{a}} = -(\gamma_a + i\Delta')\bar{a} - ig^*\overline{\sigma_{21}} + \sqrt{2\eta\gamma_a}\varepsilon_d, \tag{A1}$$

$$\dot{\bar{b}} = -(\gamma_m + iw_m)\bar{b} + iG\bar{a}^2, \tag{A2}$$

$$\dot{\overline{\sigma_{21}}} = -(\gamma_{12} + i\Delta_d)\overline{\sigma_{21}} - ig\bar{a} - i\Omega\overline{\sigma_{23}}, \tag{A3}$$

$$\dot{\overline{\sigma_{23}}} = -[\gamma_{32} + i(\Delta_d - \Delta_0)]\overline{\sigma_{23}} - i\Omega^*\overline{\sigma_{21}}. \tag{A4}$$

And each steady-state value can be obtained by setting Eqs. (A1)–(A4) to zero. Thus, we have

$$\frac{2G^2 w_m}{\gamma_m^2 + w_m^2}\bar{a}^3 + \left(\frac{g^2}{\gamma_{12} + i\Delta_d + \frac{\Omega^2}{\gamma_{32} + i(\Delta_d - \Delta_0)}} + \gamma_a + i(\Delta_d - \Delta_0)\right)\bar{a} = \sqrt{2\eta\gamma_a}\varepsilon_d, \tag{A5}$$

$$\bar{b} = \frac{iG\bar{a}^2}{\gamma_m + iw_m}. \tag{A6}$$

[1] H. Mabuchi and A. C. Doherty, Science **298**, 1372 (2002).

[2] J. McKeever, A. Boca, A. D. Boozer, R. Miller, J. R. Buck, A. Kuzmich, and H. J. Kimble, Science **303**, 1992 (2004).

[3] S. Ritter, C. Nolleke, C. Hahn, A. Reiserer, A. Neuzner, M. Uphoff, M. Mucke, E. Figueroa, J. Bochmann, and G. Rempe, Nature (London) **484**, 195 (2012).

[4] M. Aspelmeyer, T. J. Kippenberg, and F. Marquardt, Rev. Mod. Phys. **86**, 1391 (2014).

[5] F. Marquardt and S. M. Girvin, Phys. **2**, 40 (2009).

[6] T. J. Kippenberg and K. Vahala, Opt. Express **15**, 17172 (2007).

[7] J. Restrepo, C. Ciuti, and I. Favero, Phys. Rev. Lett. **112**, 013601 (2014).

[8] T. Ramos, V. Sudhir, K. Stannigel, P. Zoller, and T. J. Kippenberg, Phys. Rev. Lett. **110**, 193602 (2013).

[9] H. Ian, Z. R. Gong, Y.-X. Liu, C. P. Sun, and F. Nori, Phys. Rev. A **78**, 013824 (2008).

[10] M. Cotrufo, A. Fiore, and E. Verhagen, Phys. Rev. Lett. **118**, 133603 (2017).

[11] Y. Chang, T. Shi, Y.-X. Liu, C. P. Sun, and F. Nori, Phys. Rev. A **83**, 063826 (2011).

[12] H. Wang, X. Gu, Y.-X. Liu, A. Miranowicz, and F. Nori, Phys. Rev. A **90**, 023817 (2014).

[13] C. Jiang, L. Jiang, H. Yu, Y. Cui, X. Li, and G. Chen, Phys. Rev. A **96**, 053821 (2017).

[14] K. J. Boller, A. Imamoglu, and S. E. Harris, Phys. Rev. Lett. **66**, 2593 (1991).

[15] J. A. Souza, E. Figueroa, H. Chibani, C. J. Villas-Boas, and G. Rempe, Phys. Rev. Lett. **111**, 113602 (2013).

[16] M. Mucke, E. Figueroa, J. Bochmann, C. Hahn, K. Murr, S. Ritter, C. J. Villas-Boas, and G. Rempe, Nature (London) **465**, 755 (2010).

[17] S. Fan, Appl. Phys. Lett. **80**, 908 (2002).

[18] G. S. Agarwal and S. Huang, Phys. Rev. A **81**, 041803(R) (2010).

[19] A. H. Safavi-Naeini, T. Alegre, J. Chan, M. Eichenfield, M. Winger, Q. Lin, J. T. Hill, D. E. Chang, and O. Painter, Nature (London) **472**, 69 (2011).

[20] S. Weis, R. Riviere, S. Deleglise, E. Gavartin, O. Arcizet, A. Schliesser, and T. J. Kippenberg, Science **330**, 1520 (2011).

[21] M. Cirio, K. Debnath, N. Lambert, and F. Nori, Phys. Rev. Lett. **119**, 053601 (2017).

[22] Y. Chang, H. Ian, and C. Sun, J. Phys. B **42**, 215502 (2009).

[23] D. F. Walls and G. J. Milburn, *Quantum Optics* (Springer, Berlin, 1994).

[24] L. V. Hau, S. E. Harris, Z. Dutton, and C. H. Behroozi, Nature (London) **397**, 594 (1999).

[25] M. Fleischhauer, A. Imamoglu, and J. P. Marangos, Rev. Mod. Phys. **77**, 633 (2005).

[26] C. Weisbuch, M. Nishioka, A. Ishikawa, and Y. Arakawa, Phys. Rev. Lett. **69**, 3314 (1992).

[27] F. Massel, T. T. Heikkila, J. M. Pirkkalainen, S. U. Cho, H. Saloniemi, P. J. Hakonen, and M. A. Sillanpaa, Nature (London) **480**, 351 (2011).

[28] F. Hocke, X. Zhou, A. Schliesser, T. J. Kippenberg, H. Huebl, and R. Gross, New J. Phys. **14**, 123037 (2012).

[29] M. Liu, X. Yin, E. Ulin-Avila, B. Geng, T. Zentgraf, L. Ju, F. Wang, and X. Zhang, Nature (London) **474**, 64 (2011).

[30] A. M. Ionescu and H. Riel, Nature (London) **479**, 329 (2011).